Disentangling North Atlantic ocean-atmosphere coupling using circulation analogues

Author One[a]

[a] *First Affiliation*

Corresponding author: Author One, email@email.com

ABSTRACT: The coupled nature of the ocean-atmosphere system frequently makes understanding the chain of causality difficult in ocean-atmosphere interactions. This study presents a method to remove the component of turbulent heat fluxes which is directly forced by atmospheric circulation, diagnosing the residual as being primarily 'ocean-forced'. This method is applied to the North Atlantic in a 500-year pre-industrial control run using the Met Office's HadGEM3-GC3.1-MM model. The method identifies residual heat flux modes associated with variations in ocean circulation and shows that these force equivalent barotropic circulation anomalies in the atmosphere. The first of these modes is characterised by the ocean warming the atmosphere along the Gulf Stream and North Atlantic Current and the second by a dipole of cooling in the western subtropical North Atantic and warming in the sub-polar North Atlantic. These results tentatively suggest that the Gulf Stream may play a role in the circulation response to decadal ocean variability. More generally, this method provides a useful way to separate-out causality in ocean-atmosphere interactions which could easily be applied to other ocean basins. and to models or reanalysis datasets.

1. Introduction

The impact of extratropical sea surface temperature (SST) variability on atmospheric circulation is both a complex theoretical problem and an eminently practical one. It is a practical problem in that ocean variability is a major source of prediction skill for forecasts on sub-seasonal to decadal timescales (Meehl et al. 2021; Merryfield et al. 2020).

North Atlantic Ocean variability is thought to be an important source of climate predictability on decadal and longer timescales (Zhang et al. 2019). For example, Atlantic Multidecadal Variability (AMV) has been linked to variability in the position of the Intertropical Convergence Zone (ITCZ) and Sahel rainfall (Knight et al. 2006), multidecadal Atlantic hurricane activity (Sutton and Hodson 2007) and European climate (Sutton and Dong 2012; O'Reilly et al. 2017). On seasonal timescales, North Atlantic SST anomalies also plays some role in forcing the North Atlantic Oscillation (NAO) (Rodwell et al. 1999; Mehta et al. 2000; Czaja and Frankignoul 2002; Gastineau et al. 2013; Dong et al. 2013; Baker et al. 2019).

On the theoretical side, identifying the role of the mid-latitude SSTs in atmospheric variability presents a challenge because of the coupled nature of the ocean-atmosphere system and the relatively weak influence of the ocean on the atmosphere (Kushnir et al. 2002). On interannual and shorter timescales the atmosphere governs ocean-atmosphere covariability via modulation of air temperature, specific humidity and near-surface wind speed, and these in turn modify surface turbulent heat fluxes (Q). At decadal timescales and longer, the ocean dominates as it integrates atmospheric variability and responds via changes to ocean circulation and ocean heat transport.

Idealised modelling studies have found that the initial response to a warm mid-latitude SST anomaly consists of a linear baroclinic response, with a downstream surface low advecting cool air equatorwards to balance the heating (Hoskins and Karoly 1981; Hendon and Hartmann 1982). After around ten days, the response becomes dominated by an equivalent barotropic pattern, involving transient eddy feedbacks, with the anomalous circulation extending far beyond the initial perturbation (Deser et al. 2007). The equivalent barotropic response typically projects strongly onto the dominant modes of internal variability such as the NAO.

The circulation response to mid-latitude SSTs is substantially model dependent and is sensitive to the location of the heating relative to the mean jet. Modelled circulation responses to mid-latitude SSTs are also weak in comparison to both tropical SST-induced anomalies and internal, mid-latitude variability (Kushnir et al. 2002). However, models' responses to mid-latitude SST variability are likely too weak (Eade et al. 2014; Scaife and Smith 2018; Smith et al. 2020), possibly due to low horizontal resolution (Scaife et al. 2019) or weak eddy feedbacks (Hardiman et al. 2022). Relatedly, models underestimate the magnitude of decadal to multidecadal extratropical variability of circulation, particularly for the North Atlantic (Simpson et al. 2018; O'Reilly et al. 2021).

To identify SST-forcing of atmospheric circulation, studies use a variety of methods. These include 1) low-pass filtering data to isolate timescales at which the ocean dominates, 2) using lagged correlation analysis and 3) performing atmosphere-only experiments. However, as discussed above, current models are deficient at capturing the response to mid-latitude SSTs. Moreover, the shortness of the observed record means that low-pass filtering gives only a few degrees of freedom, while lagged correlation analysis of a short time series can be hard to interpet.

This study presents a method to separate the ocean-forced component of Q from the circulation-forced component. The method has been designed such that it does not require any low-pass filtering and can be applied to both models and reanalysis data. In this study the method is only applied to model data as this provides a more controlled setup in which there is a long data record and there is no observational uncertainty associated with variables such as Q. Testing with reanalysis data is reserved for a future paper. The method involves the use of circulation analogues to identify the component of Q directly associated with circulation variability, diagnosing the ocean-forced component as the residual. We apply this method to a 500-year pre-industrial control (piControl) run with no external forcing, before applying it to simulations of the same model with observed external forcings from 1850 to 2014.

The datasets and method are described in section 2 before the method is applied to a piControl simulation in section 3. The leading modes of the decomposition are examined in section 4, followed by an analysis of the circulation responses to the Q modes in section 5 and discussion of the sensivity to the presence of external forcing and length of the dataset in section 6. Finally, some discussion and conclusions are provided in section 7.

2. Data and methods

a. Data

We analyse simulations using the UK Met Office HadGEM3-GC31 model (Williams et al. 2018) for which North Atlantic ocean-atmosphere coupling has been extensively analysed (e.g. Lai et al. 2022; Khatri et al. 2022). The model consists of coupled ocean, atmosphere, land and sea-ice models. In this study, we primarily utilize the run with medium (MM) resolution in the ocean and atmosphere, but also briefly analyse the low (LL) resolution version. The 'LL' and 'MM' simulations are performed on N96 (grid-spacing of approximately 125km) and N216 (grid-spacing of approximately 60km) grids in the atmosphere, respectively. The horizontal ocean resolution is 0.25° (ORCA025) in 'MM' and 1° (ORCA1) in 'LL' but with a resolution of 0.33° from 15N to 15S. Both 'LL' and 'MM' have 75 vertical levels in the ocean and 85 in the atmosphere. The piControl runs using both versions of the model simulate AMV with a 60-80 year period, consistent with observations, however the versions differ in terms of their ocean circulation variability and atmospheric response to AMV (Lai et al. 2022). Both versions show a slightly weaker Atlantic Meridional Overturning Circulation (AMOC) at 26.5N and at sub-polar latitudes with respect to RAPID (Menary et al. 2018) and OSNAP observations (Menary et al. 2020), respectively.

b. Circulation analogues

In order to attribute Q anomalies to atmospheric or oceanic forcing, we apply a circulation analogues method similar to that used by Deser et al. (2016) and O'Reilly et al. (2017). The concept of comparing similar circulation states was first developed in the context of statistical weather prediction by Lorenz (1969) and later van den Dool (1994) and van den Dool et al. (2003). More recently, it has been used to study the degree to which atmospheric circulation trends have played a role in observed temperature trends (Cattiaux et al. 2010; Wallace et al. 2012; Deser et al. 2016).

The circulation analogues method attempts to estimate the component of a temporally and spatially varying variable, that is directly associated with changes in atmospheric circulation. In our case, we decompose Q into two components,

$$Q = Q_{CIRC} + Q_{RESIDUAL}, \tag{1}$$

where Q_{CIRC} is the circulation-related component of Q and $Q_{RESIDUAL}$, is the residual. We interpret the $Q_{RESIDUAL}$ to be predominantly ocean-forced. In principal, $Q_{RESIDUAL}$ will also vary due to radiative warming of the atmosphere, for example through externally forced radiative changes. There is no external forcing in the piControl run, but we remove the effects of external forcing when applying the method to historical simulations by regressing out the global-mean SST. This is discussed further in section 14. We also perform a linear detrending of piControl anomalies prior to reconstructing SLP, in order to remove any drifts in the model.

Our method begins by taking the linearly detrended, monthly-mean sea level pressure (SLP) anomalies for a particular month, say January 1901, and calculating the Euclidian distance between this month and all other Januaries over the North Atlantic region. Note that each month is only compared to its corresponding month (Januaries with Januaries etc), hence removing the seasonal cycle. A sub-sample of size N_r from the N_s most similar Januaries is then taken and this sample of anomaly maps is used to reconstruct the original (January 1901) anomaly field via a multiple linear regression, over a particular region. This gives a set of N_r weights for each of the sub-sampled months. Q_{CIRC} is then calculated by summing the Q anomalies for the same years multiplied by the corresponding weights calculated for the SLP anomalies. The resampling procedure is repeated N_a times to obtain N_a reconstructions of SLP and Q_{CIRC}, which are then averaged to find a best estimate. In practice, N_r, N_s and N_a are taken to be 50, 80 and 100, respectively. This entire process is then repeated for all years in the dataset and for all calendar months of interest. For instance, if the December-January-February-March (DJFM) mean is required, the method is applied independently for December, January, February and March, before taking the average of these reconstructions.

Applying the process separately to individual months before taking the seasonal average is a critical part of the procedure as this allows for the possibility of SSTs influencing atmospheric circulation on sub-seasonal timescales. The point of the decomposition is to remove the direct influence that atmospheric circulation has on Q; for instance, through modulation of surface wind speed or the air-sea temperature difference. This downward influence is strongest when the circulation leads the Q by 10-20 days (figure 1a, Deser and Timlin 1997). The autocorrelation timescale of the atmosphere is on the order of 2-4 weeks, in contrast to SST anomalies which persist for many months (figure 1b). Consequently, SST anomalies created by stochastic atmospheric

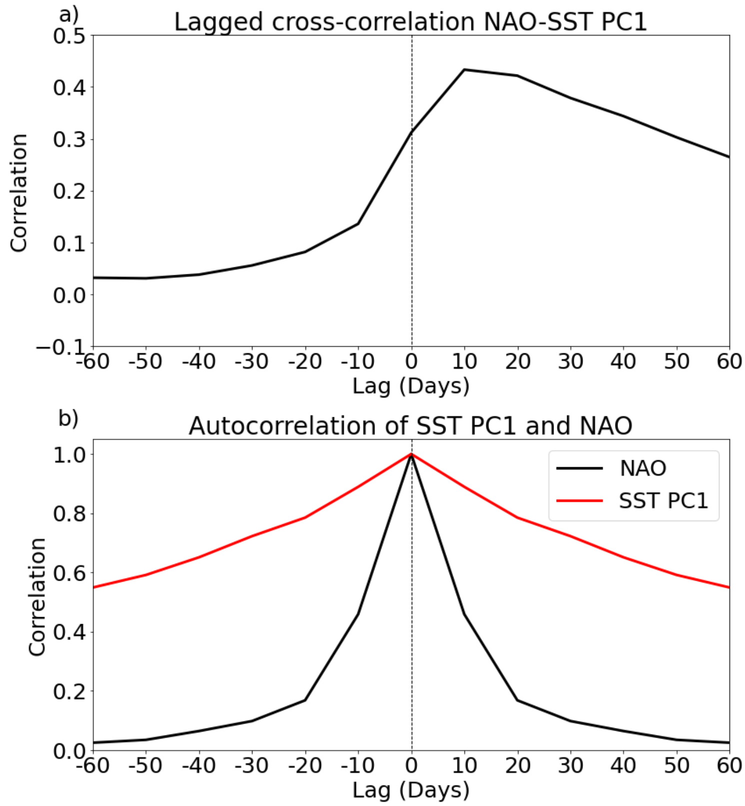

FIG. 1. a) Lagged cross-correlation of the NAO, calculated as the first principal component (PC) SLP anomalies, 20N-70N, 60W-0E, with the first principal component time series of SST, calculated over the same area for boreal winter (December-January-February-March). b) The autocorrelation of the NAO and SST PC time series'. The NAO is calculated using data from ERA5 (Hersbach et al. 2020) and the SST dataset is HadISST 2.1 (Titchner and Rayner 2014).

forcing in the early winter may then exert an influence on the atmosphere through to late winter. On the other hand, idealised experiments show that the atmospheric circulation response to mid-latitude SST anomalies takes several months to fully develop (Ferreira and Frankignoul 2005; Deser et al. 2007). Therefore, applying the method to monthly-mean data allows for circulation anomalies to develop in response to SST anomalies induced by atmospheric forcing in prior months.

The method is therefore not an attempt to completely separate the total influence of atmospheric circulation on Q, as circulation may first influence SSTs and subsequently Q. Rather, the dynamical decomposition is a diagnostic tool to measure the SST-driven component of Q and consequently, establish how patterns of SST variability affect atmospheric circulation.

c. Linear decomposition of Q anomalies

Q is composed of sensible (Q_S) and latent heating (Q_L) terms which can be represented using the bulk formulae $Q_L = \rho C_p L U \Delta H$ and $Q_S = \rho C_p C_H U \Delta T$, respectively. Here, ρ is the air density, U is the near-surface wind speed, C_p is the heat capacity of water, L is the latent heat of evaporation and C_E and C_H are transfer coefficients. $\Delta H = H_s - H_a$ and $\Delta T = T_s - T_a$ are the air-sea temperature and specific humidity differences, respectively. Here subscript s represents the sea surface and a, the atmosphere.

A linear decomposition of Q (e.g. Alexander and Scott 1997; Du and Xie 2008; He et al. 2022) yields

$$\Delta Q' = \Delta Q'_S + \Delta Q'_L \approx (\overline{Q_S} + \overline{Q_L})\frac{U'}{\overline{U}} + \overline{Q_S}\frac{\Delta T'}{\overline{\Delta T}} + \overline{Q_L}\frac{\Delta H'}{\overline{\Delta H}}, \tag{2}$$

where overbars represent time-mean quantities and primes are the anomalies with respect to the time-mean. This decomposition assumes that $U'\Delta H' << \overline{UH}$ and $U'\Delta T' << \overline{UT}$, which are both good approximations at the monthly timescale (not shown).

d. Indices

The NAO index is calculated as the first empirical orthogonal function (EOF) of DJFM-mean SLP over the region 20N-80N and 60W-0W, calculated using the python package ‘eofs’ (Dawson 2016). The AMOC index is defined, following Lai et al. (2022), as the Atlantic overturning stream function (in depth space) at 45N and 1000m depth. The AMV is calculated as the basin-mean North Atlantic SST (80W-0W, 0N-80N) after the global mean has been linearly removed from each grid-point. The index is then low-pass filtered using a 15-year running mean, again following Lai et al. (2022).

3. Applying to a piControl simulation

We now apply the circulation analogues method described in section 2 to the North Atlantic, over a box bounded by latitudes 20N-75N and longitudes 90W-0E (shown by the boxed region in figure 2). An example of the decomposition is shown in figure 2 for the winter (DJFM) of model year 1911 in the HadGEM3-GC31-MM piControl simulation. The circulation-related SLP field, marked by a postive-NAO like pattern, is by construction almost identical to the full field over the North Atlantic

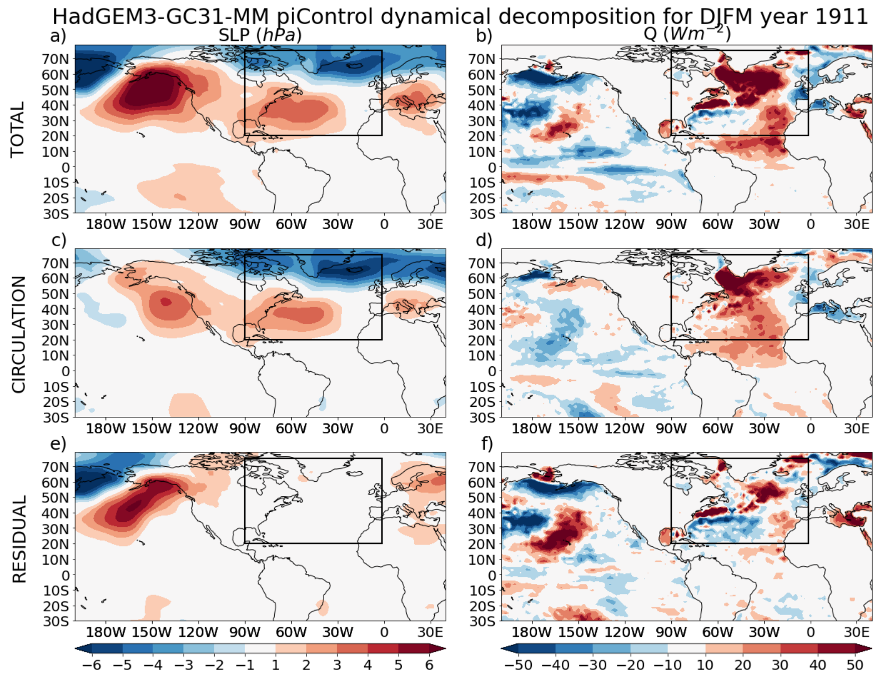

Fig. 2. Dynamical decomposition of SLP and Q anomalies for the winter (DJFM) of the year 1911 in the HadGEM3-GC31-MM piControl run.

region (figure 2a,c), however this is not the case outside of the North Atlantic (figure 2e). The Q anomalies (defined as positive upwards) indicate anomalously high heat loss from the ocean to the atmosphere over a horseshoe-shaped region involving the sub-polar North Atlantic and eastern sub-tropical North Atlantic (figure 2b). The dynamical decomposition suggests that a substantial proportion of this is related to the circulation, including heat loss over the western sub-polar and subtropical North Atlantic (figure 2d). $Q_{RESIDUAL}$ anomalies are of similar magnitude to Q_{CIRC} anomalies and are characterised by ocean heat-loss over the eastern sub-polar and heat-gain over the western subtropics, with a northward shift of the Gulf Stream (figure 2f).

Much of the sub-polar heat-loss over the sub-polar North Atlantic in winter 1911 occurs in December and January (compare figure 3d,j with figure 3p,v). Strong near-surface wind speeds and air-sea temperature and specific humidity differences all contribute to the sub-polar heat-loss (figure 3a-c, g-i), which is largely driven by atmospheric circulation (figure 3e,k). In all four months, $Q_{RESIDUAL}$ shows positive anomalies over the Gulf Stream and eastern sub-polar North Atlantic (figure 3f,l,r,x) with negative anomalies in the subtropics from January to March (figure 3l,r,x). The relative persistence of $Q_{RESIDUAL}$ compared to Q_{CIRC} across the winter, is

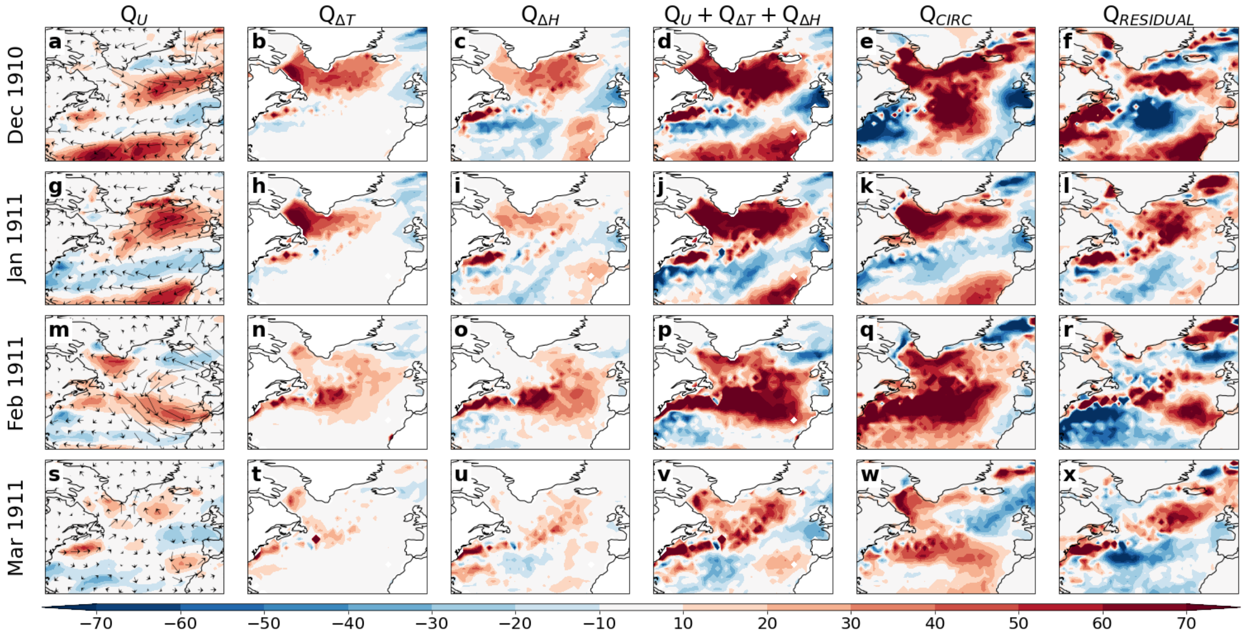

FIG. 3. Linear and dynamical decompositions of Q anomalies for the winter of model year 1911 in the piControl run. The different rows show results of the decompositions for a-f) December 1910, g-l) January 1911, m-r) February 1911 and s-x) March 1911. Columns show Q anomalies associated with a,g,m,s) surface-wind forcing, b,h,n,t) air-sea temperature differences, c,i,o,u) air-sea specific humidity differences, d,j,p,v) the sum of the first three columns, e,k,q,w) Q_{CIRC} and f,l,r,x) $Q_{RESIDUAL}$. Vectors in a,g,m,s) show 10m wind anomalies. Q anomalies are in units of Wm^{-2}.

suggestive of the role of lower frequency SST variability in $Q_{RESIDUAL}$. Nevertheless, there are distinct $Q_{RESIDUAL}$ differences between each month, possibly due to atmospheric forcing from the previous month affecting SSTs.

To test the dynamical decomposition method more systematically, we calculate the correlation, at each grid-point, between DJFM-mean SST anomalies and the components of the Q dynamical decomposition. Consider that if a warm SST anomaly is primarily the result of warming by the atmosphere, then the anomalous Q is negative, while a cool SST anomaly will be associated with a positive upward heat flux anomaly. Conversely, if the SST anomaly is warming or cooling the atmosphere, having formed through alterations to ocean circulation or by atmospheric forcing at least a month or two previous, then the sign of the SST anomaly should be the same as that of the anomalous heat flux. That is, a negative correlation between SST and Q anomalies indicates a downward influence, while a positive correlation indicates an upward influence (e.g. Gulev et al.

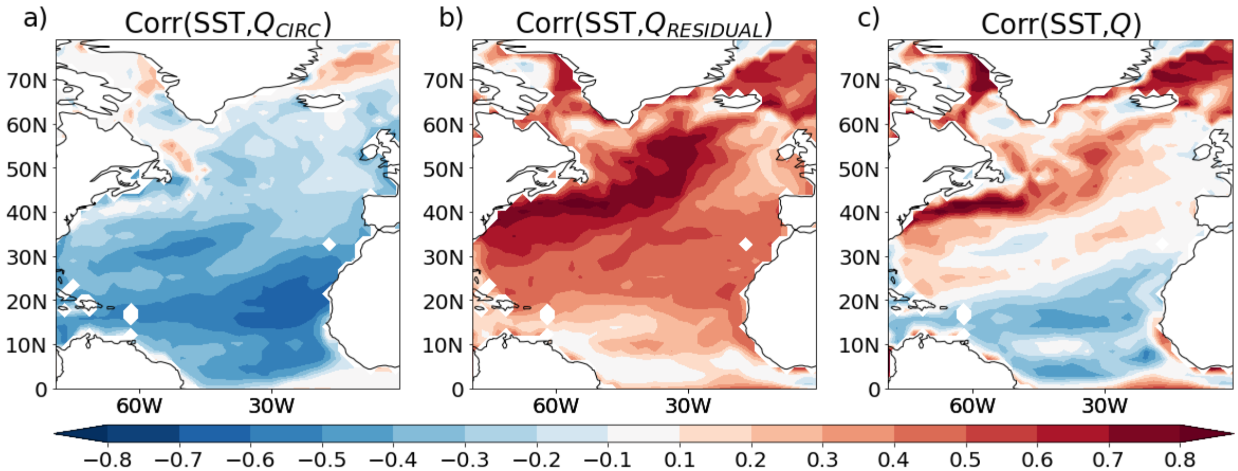

FIG. 4. Grid-point correlations between SST anomalies and a) Q_{CIRC}, b) $Q_{RESIDUAL}$ and c) Q in the HadGEM3-GC1-MM piControl run.

2013; O'Reilly et al. 2016; Bishop et al. 2017; Blackport et al. 2019; O'Reilly et al. 2023). As anticipated, the Q_{CIRC} component is negatively correlated with SST across the North Atlantic, suggesting a primarily downward influence (figure 4a). In contrast, SSTs are positively correlated with the $Q_{RESIDUAL}$ (figure 4b), suggesting a largely upward influence of Q anomalies. For reference, the full Q field shows that over the extratropical North Atlantic, SST variability tends to warm the atmosphere more so than the atmosphere warms the SSTs, whereas the influence is generally downward in the tropical Atlantic (figure 4c). Unsurprisingly, Q variability in the Gulf stream region stands out as being particularly dominated by the ocean (figure 4c, figure 5c).

The majority of modelled Q variability in the sub-polar North Atlantic and particularly the Labrador Sea, is associated with Q_{CIRC} (figure 5a,c). This may be due to circulation modulating the advection of cold air from the North American continent over the ocean, raising the air-sea temperature constrast. Nevertheless, the $Q_{RESIDUAL}$ shows a similar magnitude of variability to Q_{CIRC} along the North Atlantic Current (NAC) and larger variability associated with the Gulf Stream region. Therefore, while Q_{CIRC} variability is larger over the sub-polar region, neither component of the decomposition completely dominates the Q variability over the extratropical North Atlantic. The next section examines the primary modes of Q variability associated with the components of the Q decomposition and relates these to patterns of atmospheric circulation.

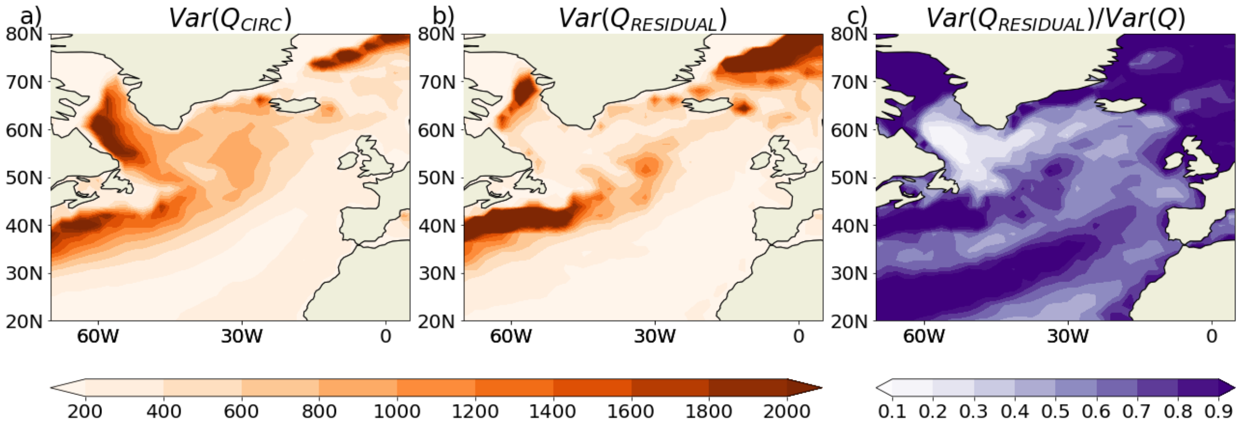

FIG. 5. Variance associated with interannual (DJFM) variability of components of the Q decomposition. Shown is the variance in a) Q_{CIRC}, b) $Q_{RESIDUAL}$ and c) the ratio of the variance of $Q_{RESIDUAL}$ to the variance in Q. Units for a,b) are both $(Wm^{-2})^2$ and c) is unitless.

4. Modes of Q variability

To understand the spatial patterns of variability associated with the Q decomposition, we perform an area-weighted EOF analysis separately for Q, Q_{CIRC} and $Q_{RESIDUAL}$, over the same region used to calculate the decomposition (20N-75N, 60W-0E). The EOFs 1 and 2 of both Q and Q_{CIRC} are characterised by a tripole pattern (figure 6a,e), associated with the positive phase of the NAO (figure 6c,g) and enhanced Q over the central North Atlantic (figure 6b,f), linked to the East Atlantic Pattern (figure 6d,h), respectively. The first two EOFs of Q_{CIRC} explain more variance (EOF1: 34.5%, EOF2: 17.5%) than those of Q (EOF1: 25.0%, EOF2: 12.6%) because Q also includes variability which is unrelated to atmospheric circulation.

EOF1 and EOF2 of $Q_{RESIDUAL}$ are more spatially localised, instead marked by anomalous positive Q along the NAC (figure 6g) and positive Q anomalies to the south-east of Greenland, with a weak negative anomaly in the subtropics. $Q_{RESIDUAL}$ EOF1 is somewhat reminiscent of the 'slow' response at 3-4 year lags to NAO forcing found by Khatri et al. (2022) in using the same model but with decadal hindcast data (c.f. their figure 2). They found that the initial 'fast' response to the NAO caused by wind stress and Q anomalies is followed by a slower adjustment to SSTs involving a strengthened overturning circulation, as shown in figure 7c). This is corroborated by the fact that lagged correlations between the NAO and PC1 peak when the NAO leads by one year (figure 7a).

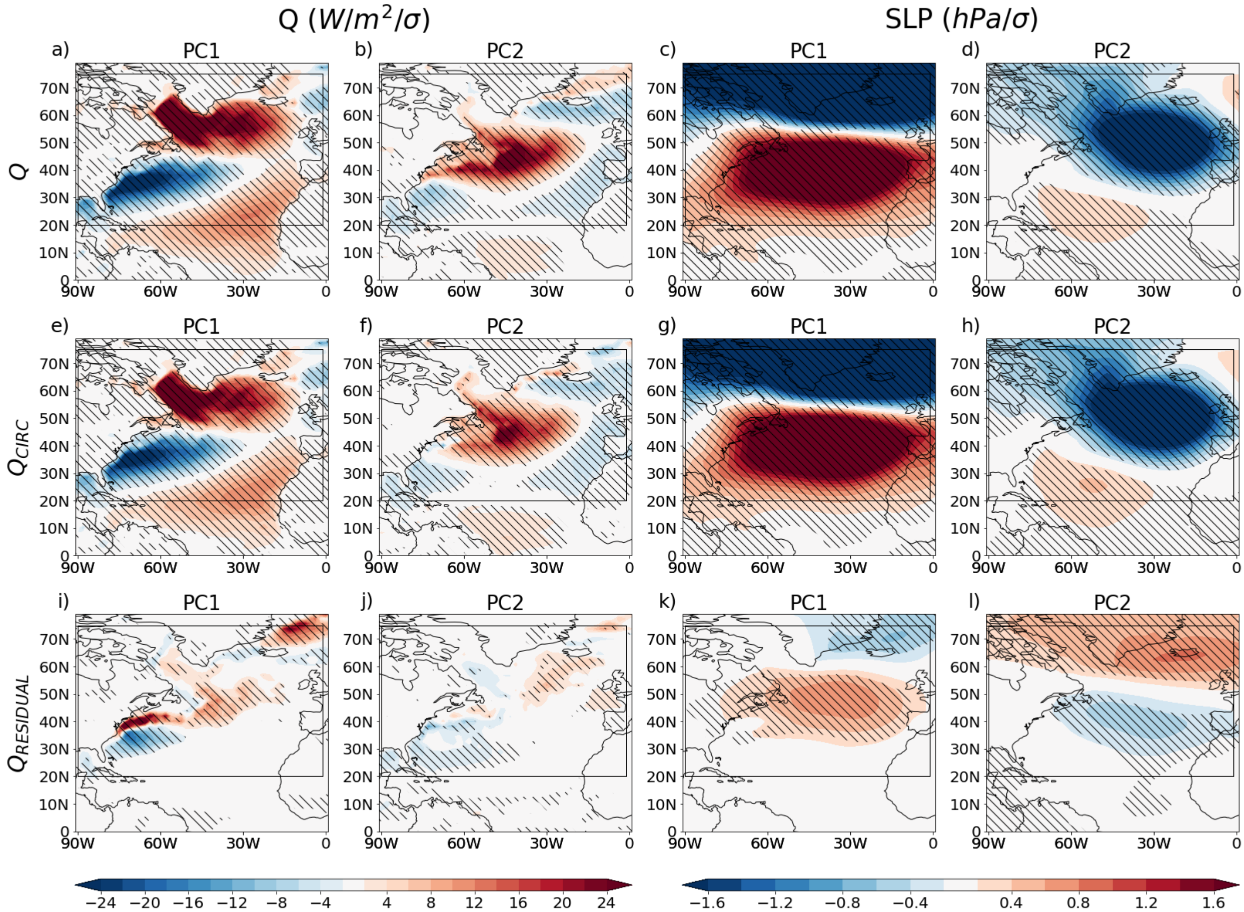

FIG. 6. Leading modes of variability associated with the components of the Q decomposition. The first and second EOFs of a-d) Q, e-h) Q_{CIRC} and i-l) $Q_{RESIDUAL}$ are shown regressed onto a-b,e-f,i-j) Q and c-d,g-h,k-l) SLP. Hatching indicates where regression coefficients are statistically significant at the 95% level following a t-test. The boxed region indicates the region over which both the decomposition and EOFs are calculated.

Lagged correlation / regression analysis shows that the AMOC begins to strengthen about five years prior to the maximum of $Q_{RESIDUAL}$ PC1 (figures 7b, 8b). It is likely that this AMOC variability represents the integration of NAO variability over multiple years (e.g. O'Reilly et al. 2019). The signature of lower frequency, ocean variability is also seen in the power spectrum of $Q_{RESIDUAL}$ PC1, which has notable peaks for periods of 20 and 40 years, neither of which is seen for Q and Q_{CIRC} (figure 8c,d).

Interestingly, $Q_{RESIDUAL}$ PC2 shows a strengthened AMOC ten years before the PC2 peak (figures 7e), with the maximum $Q_{RESIDUAL}$ PC2-AMOC correlation occurring when the AMOC

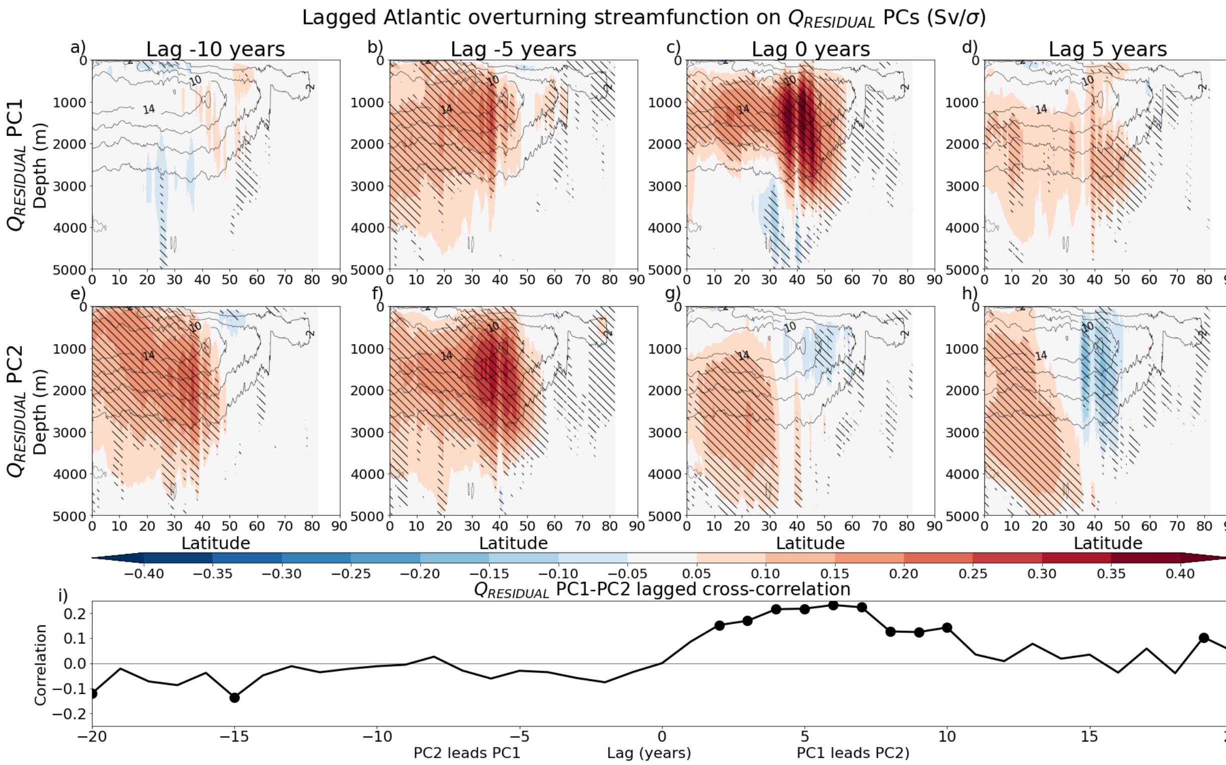

FIG. 7. Lagged regression of $Q_{RESIDUAL}$ PC time series' associated with a-d) EOF1 and e-h) EOF2 with the Atlantic overturning stream function (colours) as a function of depth and latitude. The mean overturning stream function is shown by unfilled contours with contours drawn every 4Sv, beginning at 2Sv. Hatching indicates statistically significant where regression coefficients are statistically significant following a t-test. i) Shows results of a lagged correlation analysis between $Q_{RESIDUAL}$ PC1 and PC2 with PC1 leading at positive lags. Filled circles indicate statistically significant correlations following a t-test.

leads by 5-7 years (figure 8b). This is likely because $Q_{RESIDUAL}$ PC2 to some extent reflects a continuation of PC1, as the two are significantly correlated when PC1 leads by 3-10 years. Physically, warm SST anomalies associated with $Q_{RESIDUAL}$ PC1 propagate polewards towards the eastern sub-polar North Atlantic (figure 9) on timescales of 4-6 years. This timescale is roughly consistent with observations (Årthun and Eldevik 2016; Årthun et al. 2017) and analysis of an earlier version of HadGEM3 (Menary et al. 2015).

In summary, positive $Q_{RESIDUAL}$ PC1 events are preceded by positive NAO forcing in the previous years which cools the western sub-polar North Atlantic and warms the Gulf Stream region (as indicated by Q_{CIRC} in figure 9). These changes drive a stronger AMOC and warm SSTs along

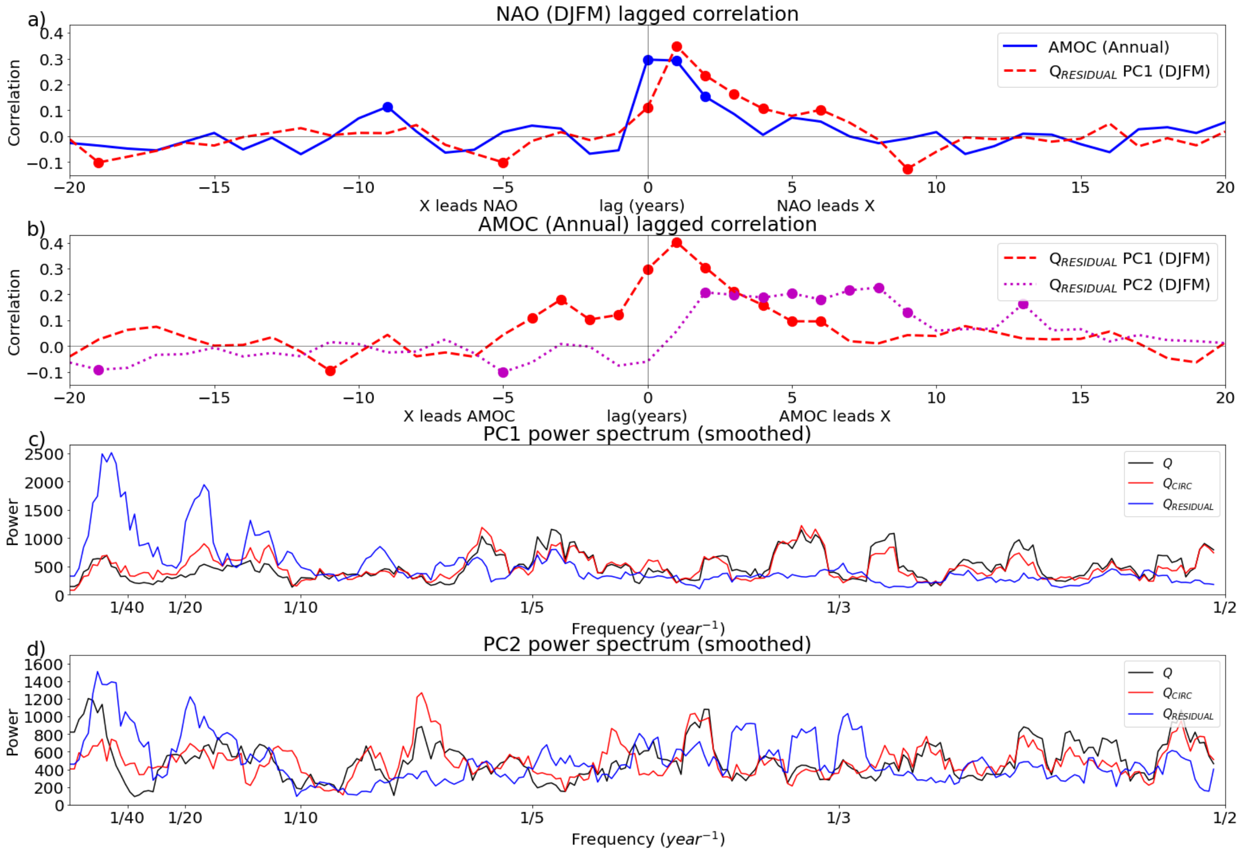

FIG. 8. Lagged correlations for a) the NAO index with the AMOC and $Q_{RESIDUAL}$ PC1, b) the AMOC with $Q_{RESIDUAL}$ PC1 and PC2. Filled circles indicate statistically significant correlations following a t-test. Power spectra are also shown for the c) first and d) second principal components of Q (black), Q_{CIRC} (red) and $Q_{RESIDUAL}$ (blue).

the NAC (figure 7b,9). These SST anomalies force an Atlantic ridge response, which is investigated in the next section. The SST anomalies subsequently propagate towards the eastern sub-polar North Atlantic. $Q_{RESIDUAL}$ PC2 events follow $Q_{RESIDUAL}$ PC1 events 3-10 years later, with the North Atlantic now marked by warm sub-polar and cool Gulf Stream regions. This subsequently forces a negative NAO, which is also investigated in the next section.

5. Circulation response to heat flux anomalies

Both $Q_{RESIDUAL}$ PC1 and PC2 are correlated with SLP anomalies at zero lag, suggesting that these are a response to the anomalous Q as the direct circulation-forced component of Q has been removed from $Q_{RESIDUAL}$ by construction. $Q_{RESIDUAL}$ PC1, which is associated with positive

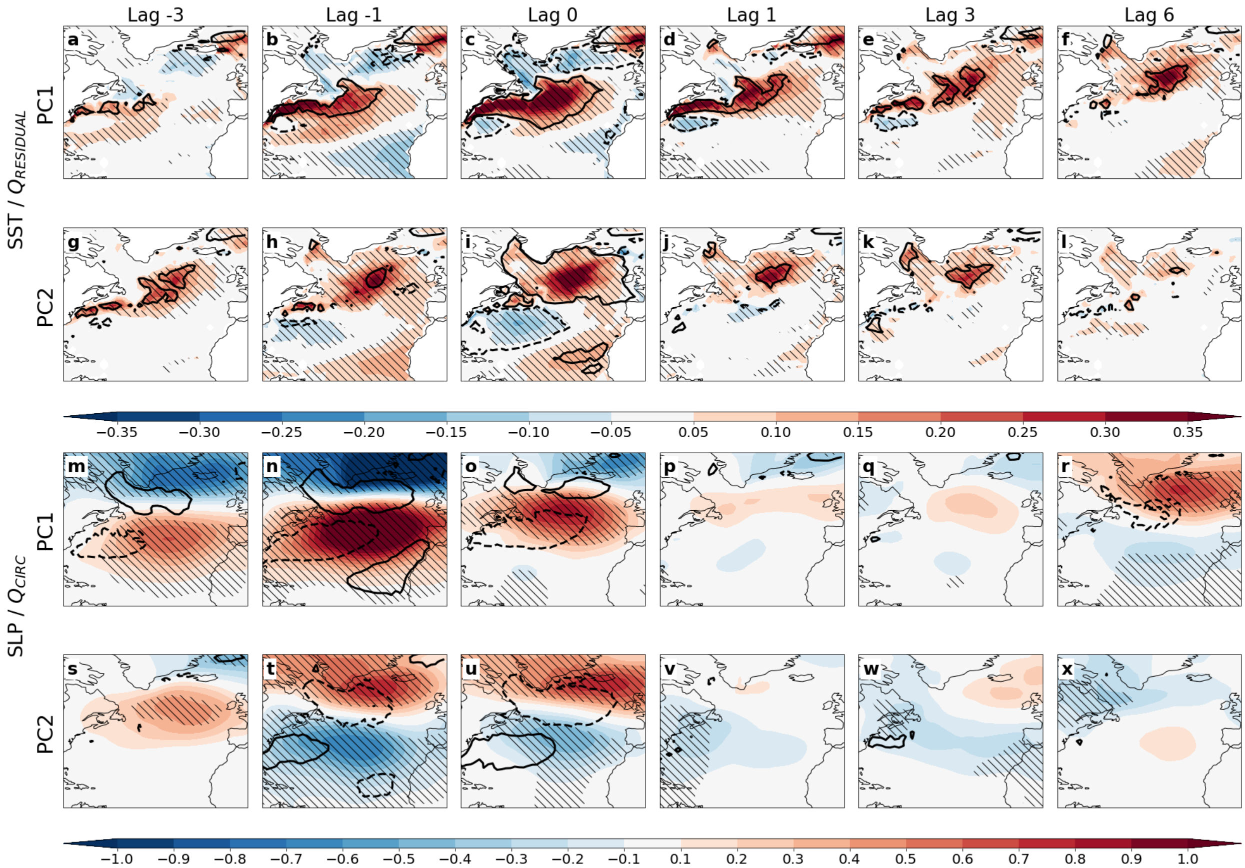

FIG. 9. Lagged regression with $Q_{RESIDUAL}$ PC1/PC2 with SST and SLP in colours and $Q_{RESIDUAL}$ and Q_{CIRC} shown by unfilled contours. For $Q_{RESIDUAL}$ and Q_{CIRC}, contours are only drawn for $\pm 3Wm^{-2}$ for visual clarity. Hatching indicates where SST / SLP regression coefficients are statistically significant at the 95% level following a t-test. The lagged cross-correlation between $Q_{RESIDUAL}$ PC1 and PC2 is also shown, with filled scatter points indicating that the correlations are statistically significant at the 95% level, also following a t-test.

SSTs along the NAC (figure 10a), forces a ridge between 40N and 60N, with an opposite-signed anomaly east of Greenland (figure 6). This is also linked to an equivalent-barotropic northward shift of the jet and strengthening of storm track activity in the western North Atlantic, measured using transient heat transport, $v'T'$, as a proxy (figure 10b,c). The primes indicate high-pass filtering with a 10-day Lanczos filter (Duchon 1979). The increase in storm track activity is likely driven by the increased SST gradient along the northern flank of the Gulf Stream (figure 10a) and hence increased baroclinicity. The paradigm of Novak et al. (2015) suggests that periods of high transient heat transport are associated with a higher frequency of downstream wave-breaking

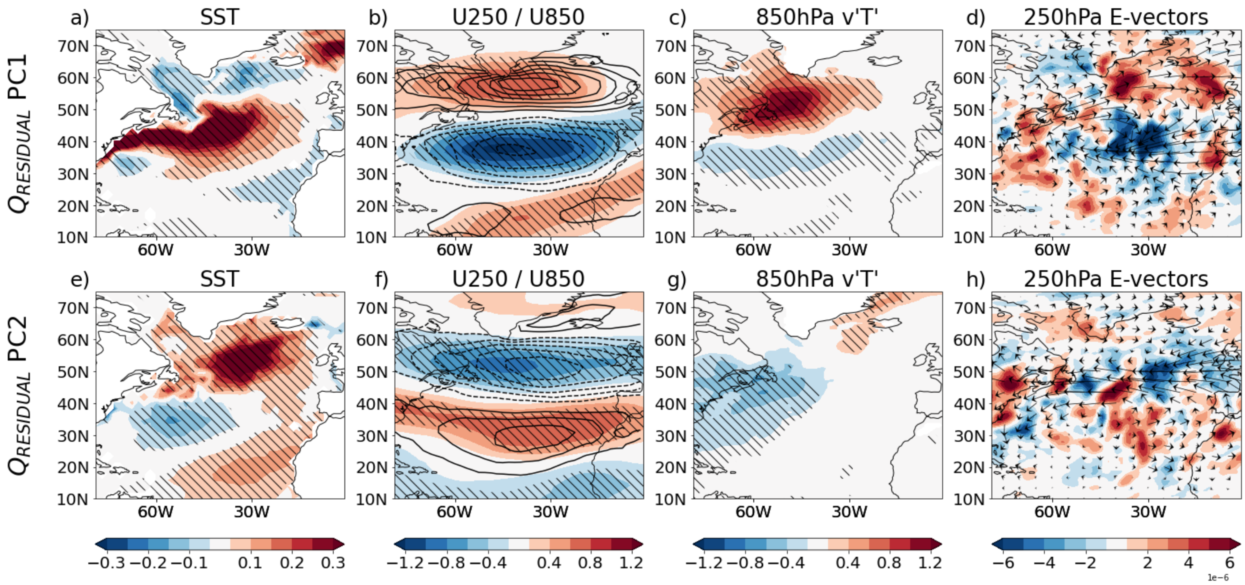

FIG. 10. Diagnostics showing the circulation response to $Q_{RESIDUAL}$ a-d) EOF1 and e-h) EOF2. Shown are regressions of the $Q_{RESIDUAL}$ PC1 and PC2 indices with a,e) SSTs, b,f) 250hPa (colours) and 850hPa (unfilled contours) winds, c,g) 850hPa 10-day high pass filtered meridional heat transport at 850hPa, d,h) E vectors (vectors). Colours in d,h) indicate the divergence associated with those vectors. Unfilled contours in b,f) are contoured every $0.1 ms^{-1}/\sigma$. Hatching indicates statistically significant where regression coefficients are statistically significant following a t-test.

on the southward side of the jet. This decelerates the jet on the equatorward flank and transfers momentum poleward (as indicated by the divergence of E-vectors in figure 10d), deflecting the jet polewards. In contrast, $Q_{RESIDUAL}$ PC2 forces a negative NAO-like pattern (figure 6) and an equatorward shift of the eddy-driven jet. Understanding the response to PC2 is complicated by the presence of two centres of action in the $Q_{RESIDUAL}$ pattern - one over the sub-polar North Atlantic and another in the Gulf Stream region (figure 6j). The transient heat transport response for PC2 is slightly weaker than for PC1, but it is possible that the cooler Gulf Stream in PC2 acts to shift the jet southward via a similar mechanism to PC1 (but with signs reversed).

To further interrogate the relative importance of the different centres of action, we regress $Q_{RESIDUAL}$ and SLP onto the NAO and onto the mean $Q_{RESIDUAL}$ calculated over boxes in the eastern sub-polar (50N-60N,40W-20W), sub-tropical (25N-35N,55W-40W) and NAC (40N-50N,40W-30W) regions. The response to PC2 is NAO-like, hence it is surprising that the NAO-

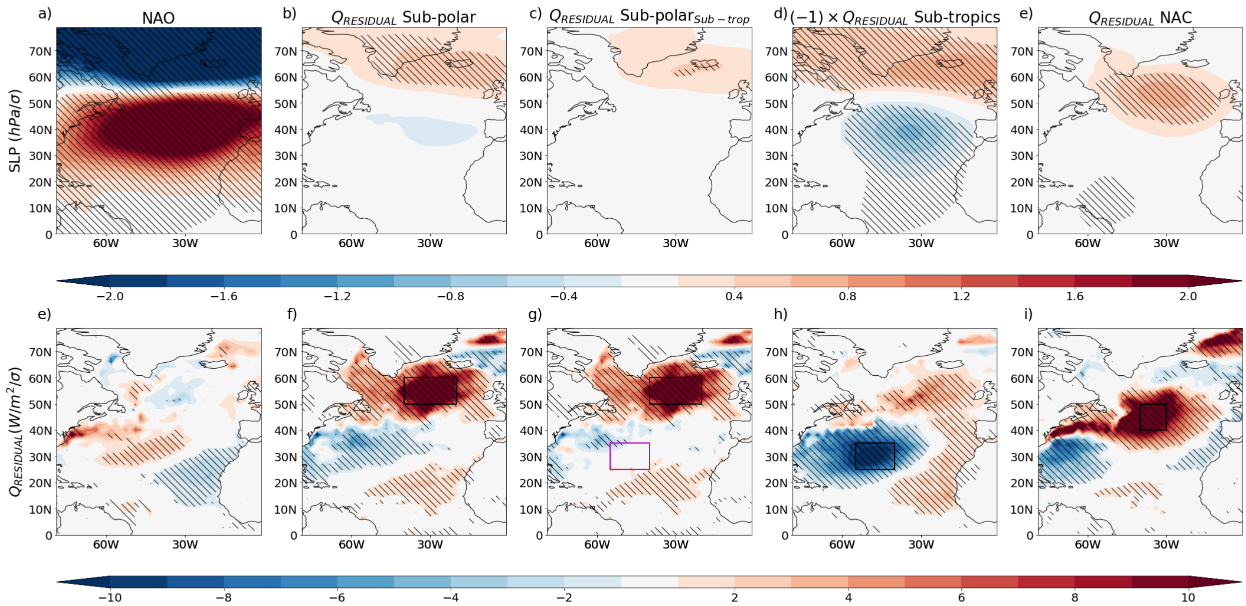

FIG. 11. Regression analysis of the connection between SLP and $Q_{RESIDUAL}$ variability in the piControl run. Regression of the NAO index onto a) SLP and e) $Q_{RESIDUAL}$. The other panels show regression of b-d) SLP and f-h) $Q_{RESIDUAL}$ onto the mean $Q_{RESIDUAL}$ in boxes over the b,f) sub-polar (50-60N,40W-20W) c,g) subtropical (25-35N,55W-40W) and d,g) NAC (40-50N, 40W-30W) regions. Each of these regions is indicated by boxes in the respective panels. Hatching in a-h) indicates where regression coefficients are statistically significant at the 95% level following a t-test.

$Q_{RESIDUAL}$ regression shows near zero regression coefficients over the eastern sub-polar North Atlantic (figure 11e), which features prominently in PC2 (figure 6j). Similarly, anomalously high $Q_{RESIDUAL}$ over the eastern sub-polar North Atlantic shows little connection with circulation variability (figure 11b,f). In contrast, negative sub-tropical $Q_{RESIDUAL}$ anomalies are linked to a negative NAO-like pattern (figure 11c,g), similar to $Q_{RESIDUAL}$ PC2 (figure 6l). This suggests that it is the sub-tropical / Gulf Stream region which forces the response to $Q_{RESIDUAL}$ PC2 with the sub-polar North Atlantic playing little role. This is consistent with Baker et al. (2019) who found the NAO to be sensitive to SST variability in the western subtropical North Atlantic (see their figure 1). For completeness, high $Q_{RESIDUAL}$ along the NAC, as in PC1, forces a similar pattern to PC1 (compare figure 6k with figure 11d,h), suggesting that the warm NAC is indeed forcing the ridge over the North-east Atlantic.

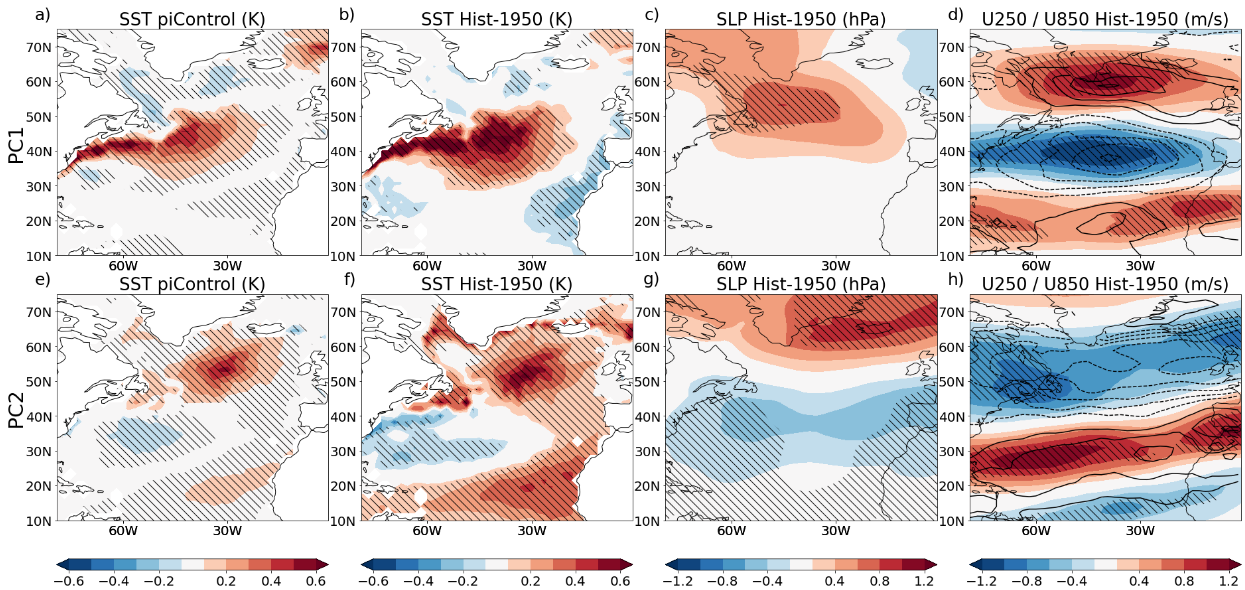

FIG. 12. Regressions of SSTs onto $Q_{RESIDUAL}$ EOFs 1 and 2 in the piControl run and regressions of SST, SLP and U850 onto an index of SST variability in Hist-1950 experiments. The index is the projection of the SSTs in the Hist-1950 onto SST patterns associated with $Q_{RESIDUAL}$ EOFs 1 and 2 in the piControl simulation. Hatching indicates where regression coefficients are statistically significant at the 95% level following a t-test.

Further evidence that the circulation patterns correlated with the $Q_{RESIDUAL}$ PCs are forced by the SSTs is provided by analysis of atmosphere-only simulations. The atmosphere-only simulations, entitled Hist-1950, are run using the same model, but forced with observed SSTs and historical greenhouse gas and aerosol forcings spanning 1950-2014. The SSTs do not react to changes in circulation patterns and hence the direction of causality is clear. There are three ensemble members of Hist-1950 and we take the ensemble average as the SSTs are the same in each case. We project the SST patterns associated with $Q_{RESIDUAL}$ PC1 and PC2 onto SSTs in the Hist-1950 simulations, over the North Atlantic box used for the dynamical decomposition (20N-75N,60W-0W), and regress SSTs, SLP and zonal wind onto the resulting time series. The piControl and Hist-1950 SST patterns show a reasonable remsemblance (figure 12a,b and figure 12e,f), though the correspondence is imperfect as the Hist-1950 run is forced by observed SSTs, which will have different modes of SST variability. Similar to the piControl simulations, the $Q_{RESIDUAL}$ PC1 pattern is associated with a high SLP anomaly over the extratropical North Atlantic, albeit with its centre shifted slightly further west in Hist-1950. The $Q_{RESIDUAL}$ PC2 pattern also shows a similar

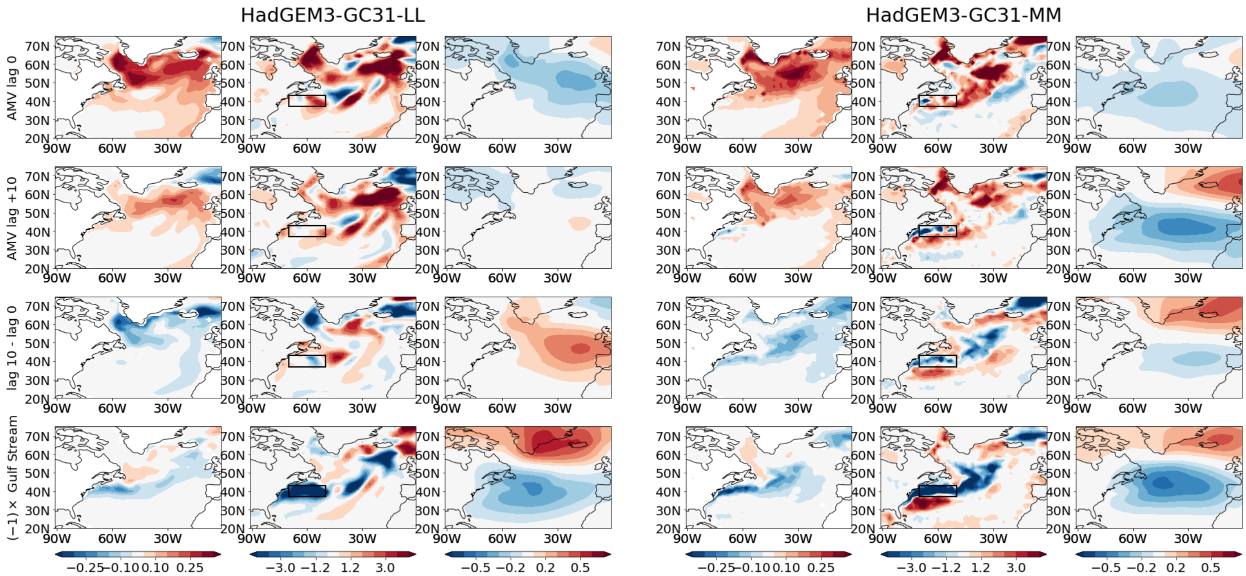

FIG. 13. Variables regressed onto AMV in the (left) LL and (right) MM versions of HadGEM3-GC3.1. Shown are regressions of 15-year running mean SST,$Q_{RESIDUAL}$ and SLP onto (top) AMV at lag 0, (middle) the AMV index but for the AMV leading by 10 years, (middle) the difference of these (AMV lag 10 minus lag 0) and (bottom) a Gulf Stream index (see text). The box used to define the Gulf Stream index is shown in panels with $Q_{RESIDUAL}$ regressions.

response in Hist-1950 to the piControl, in both cases being characterised by a negative NAO-like pattern.

As a final application of the dynamical decomposition method, we analyse the response of HadGEM3-GC3.1 to AMV with differing horizontal resolutions. Lai et al. (2022) showed that the MM version of the model exhibits a negative NAO response following a positive AMV event, while the LL version shows little response (figure 13). For zero lag, both LL and MM versions have the characteristic horseshoe-like SST pattern of AMV and are associated with negative SLP anomalies in the North Atlantic. The negative SLP anomalies are may be associated with the circulation pattern driving the AMV in the first place (whether directly via surface heat fluxes or indirectly via changes to AMOC strength). Ten years after the AMV peak, the LL and MM SST patterns are relatively similar with one difference being in the Gulf Stream region, where MM shows a weak negative SST anomaly. Given their similarity, what is the cause of the difference in circulation responses to AMV?

Regressions with $Q_{RESIDUAL}$ reveal more of a difference between the LL and MM simulations at lag 10, again particularly in the Gulf Stream region. The MM run shows a negative $Q_{RESIDUAL}$ anomaly at lag 10 in the boxed region, whereas the LL simulation shows no substantial anomaly. The SST differences between lag 10 and lag 0 for the LL and MM runs again emphasise this difference between the model versions, with a clear difference in the Gulf Stream SST for MM, but none for LL. To provide further evidence that the Gulf Stream anomalies are the reason for the difference in responses to AMV between the different versions, we compute a Gulf Stream index as the mean $Q_{RESIDUAL}$ within the boxed region shown in figure figure 13 (70W-50W,37N-43N) and regress the variables onto this index. For both LL and MM versions, this produces an SLP pattern similar to the AMV lag 10 for MM, with a low pressure anomaly in the mid-latitudes and high pressure north-west of the UK. This is also akin to the observed response to Gulf Stream SST identified by Wills et al. (2016). This analysis suggests that rather than AMV primarily influencing atmospheric circulation via the sub-polar North Atlantic, that it is the Gulf Stream region which plays a leading role, at least in HadGEM3-GC3.1.

6. Sensitivity to period length and external forcing

This study has presented the results of applying the circulation analogues method to a piControl run with a long time series and no externally forced variability. It would however be desirable to apply this to historical simulations or reanalysis datasets which are shorter and are subject to variations in greenhouse gases and aerosols. This next section therefore investigates the sensitivity of the method to the length of the period and presence of external forcing. To test the sensitivity to the length of the time period, we perform the dynamical decomposition using five 100-year and three 165-year, non-overlapping subsets of the piControl run. We also apply the dynamical decomposition to a four-member ensemble of runs with observed external forcings spanning 1850-2014 (historical), which have been created using the same model. In each case, the same values of N_r, N_a and N_s are used as for the original piControl run. For the historical simulations, the influence of external forcing is removed by linearly regressing out the global-mean SST from all variables before performing the dynamical decomposition.

Figure 14 shows the sensitivity of the NAO to forcing by anomalous $Q_{RESIDUAL}$, as in figure 11e), but calculated using subsets of the piControl run and for historical simulations. The 165-

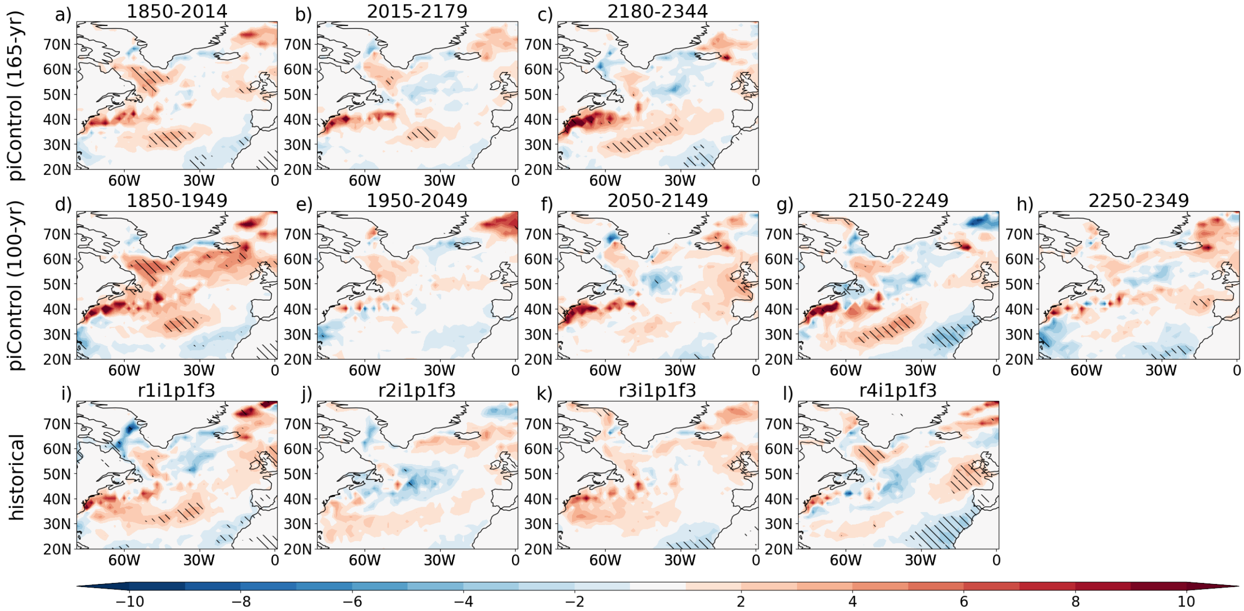

FIG. 14. Uncertainty associated with calculating SST forcing of the NAO using shorter periods of data. Results of regressing $Q_{RESIDUAL}$ onto the NAO are shown for a-c) the piControl run split into three 165-year periods, d-h) the piControl run split into five 100-year periods and i-l) four historical runs using the same model. Hatching indicates where regression coefficients are statistically significant at the 95% level following a t-test. Units are $W/m^2/\sigma$.

year subsets of the piControl are similar to one another and to the results from the full 500-year period. For instance, all show the positive phase of the NAO to be linked to anomalously high $Q_{RESIDUAL}$ over the Gulf Stream, a centre of action at 40W,30N and over the Labrador sea (figure 14a-c). The 100-year subsets are also broadly similar to one another, but the strength of the different centres of action varies considerably between periods. The 1850-1949 and 2150-2249 periods show a relatively strong forcing of the NAO from the region around 40W,30N, but this correspondence is much weaker and not significant in the other periods (figure 14d-h). Similarly, the historical simulations show roughly similar patterns overall, again with positive NAO-$Q_{RESIDUAL}$ correlations around 40W,30N and over the Labrador sea, but with the strength of the connection varying considerably between runs.

Performing the EOF analysis of $Q_{RESIDUAL}$ as before, the historical simulations each show similar dominant patterns of $Q_{RESIDUAL}$ variability to the piControl, though for ensemble members r1i1p1f3 and r2i1p1f3 the order of the first two PCs is flipped. This suggests that external forcing

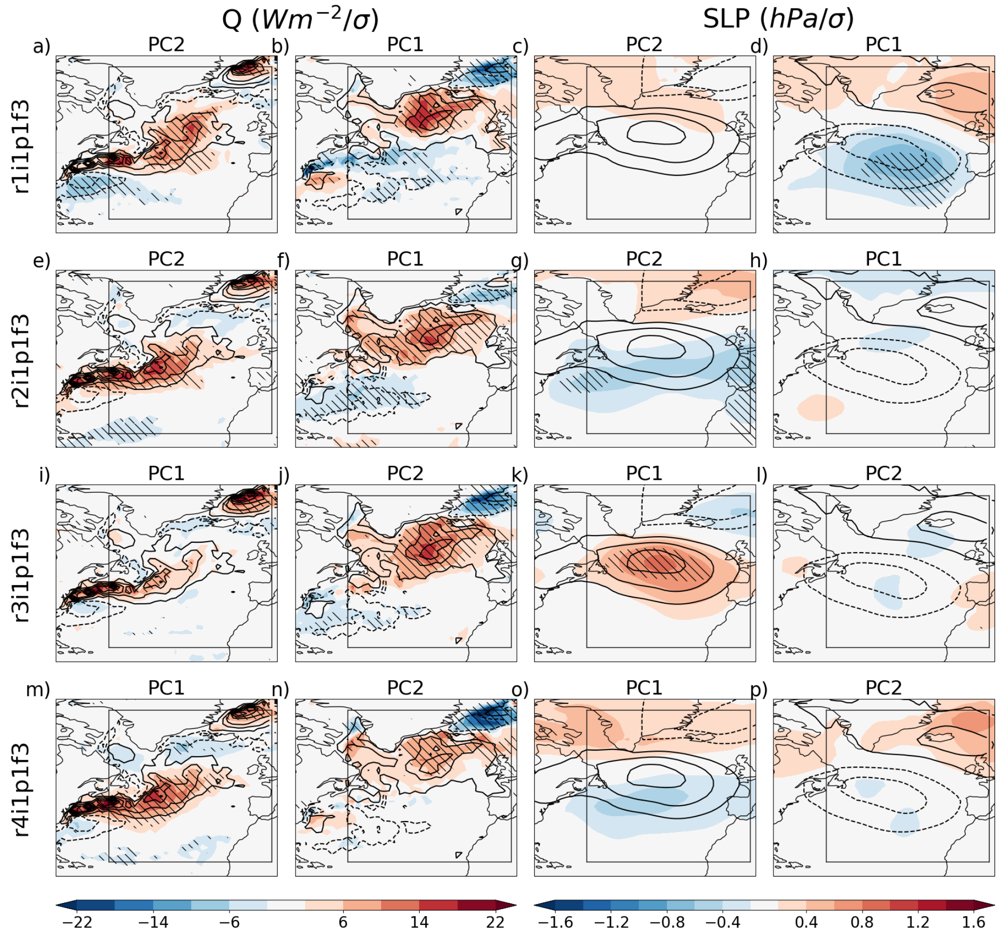

FIG. 15. Regressions of Q and SLP onto the first two PCs of $Q_{RESIDUAL}$ for the four historical ensemble members is shown by colours with the results from the piControl simulations shown by unfilled contours. Hatching indicates where regression coefficients are statistically significant at the 95% level following a t-test.

and the shorter length of the simulations does not prevent identification of the leading modes by which SST impacts the atmosphere. Further, this provides further evidence that the dynamical decomposition could usefully be applied to reanalysis datasets, which have the added complexity of external forcing and are considerably shorter than a typical piControl run. However, only r1i1p1f3 PC1, r3i1p1f3 PC1 and r4i1p1f3 PC2 show similar SLP responses to the piControl and indeed r2i1p1f3 PC2 and r4i1p1f3 PC1 show opposite responses, suggesting that the SLP response to the $Q_{RESIDUAL}$ modes is either non-stationary or overwhelmed by internal variability for the shorter simulations.

7. Discussion and conclusions

This study has presented a method to remove the direct effects of atmospheric circulation on Q and thus reveal a residual component of Q, $Q_{RESIDUAL}$, which is forced by SSTs. The method uses a circulation analogues technique and has been tested using the HadGEM3-GC3.1-MM piControl run for the wintertime North Atlantic. The leading modes of $Q_{RESIDUAL}$ show substantial low frequency variability and the peak of the EOF1 is closlely linked with a strengthening of the AMOC. The modes are characterised by a warming of the atmosphere along the Gulf Stream and North Atlantic Current for the EOF1; and a dipole of Q anomalies with cooling of the atmosphere in the western subtropical North Atlantic and warming in the eastern sub-polar region for EOF2. The first and second modes also drive equivalent barotropic atmospheric circulation responses in the form of Atlantic ridge and negative NAO patterns, respectively.

Although beyond the scope of this paper, it would be of interest to apply this method to other regions. For example, Indian Ocean SSTs are strongly affected by atmospheric variability, but also can force atmospheric circulation anomalies. Hence, the dynamical decomposition could provide a useful diagnostic for separating the atmospheric and ocean-driven Q patterns in this region. Other regions which could be of interest include the tropical Atlantic and North Pacific.

It should be noted that the dynamical decomposition method is primarily a diagnostic tool, for separating atmospheric and ocean-driven components of Q. That is to say, the atmosphere responds to Q and not $Q_{RESIDUAL}$. O'Reilly et al. (2023) identified differences in the sign of Q anomalies in free-running, coupled model experiments compared with idealised pacemaker experiments. Specifically, restoring tropical Atlantic SSTs towards particular patterns often results in positive Q, though in coupled runs, warm SSTs in this location are usually linked negative Q. The dynamical decomposition method could be of particular use in comparing Q in free-running models to that in pacemaker experiments and thus establishing whether the SST-restoring primarily occurs through atmospheric or oceanic adjustment.

This study has also shown that shorter historical simulations, forced by variable greenhouse gases and aerosols, using the same model as for the piControl simulation, produce similar $Q_{RESIDUAL}$ patterns to the piControl. However, the atmospheric circulation response shows considerably more uncertainty in the historical runs. Mid-latitude SST variability which appreciably affects atmospheric circulation, primarily occurs on decadal to multidecadal timescales as the forcing itself is weak and must therefore be persistent. Hence, even for a 100-year dataset, this may be inadequately sampled. This would therefore suggest that caution should be exercised in studying the circulation response in shorter model runs or reanalyses datasets. Nevertheless, there is significant evidence that the real-world response to mid-latitude SSTs is underestimated in models (Eade et al. 2014; Scaife and Smith 2018; Smith et al. 2020) and that models underestimate the true multidecadal variability of North Atlantic circulation (Simpson et al. 2018; O'Reilly et al. 2021) and hence 100-year long reanalysis datasets may still show an appreciable signal. We aim to examine this in a future paper.

Acknowledgments.

Data availability statement.

References

Alexander, M. A., and J. D. Scott, 1997: Surface Flux Variability over the North Pacific and North Atlantic Oceans. *Journal of Climate*, **10 (11)**, 2963–2978, https://doi.org/10.1175/1520-0442(1997)010<2963:SFVOTN>2.0.CO;2, URL https://journals.ametsoc.org/view/journals/clim/10/11/1520-0442_1997_010_2963_sfvotn_2.0.co_2.xml, publisher: American Meteorological Society Section: Journal of Climate.

Baker, H. S., T. Woollings, C. E. Forest, and M. R. Allen, 2019: The Linear Sensitivity of the North Atlantic Oscillation and Eddy-Driven Jet to SSTs. *Journal of Climate*, **32 (19)**, 6491–6511, https://doi.org/10.1175/JCLI-D-19-0038.1, URL https://journals.ametsoc.org/view/journals/clim/32/19/jcli-d-19-0038.1.xml, publisher: American Meteorological Society Section: Journal of Climate.

Bishop, S. P., R. J. Small, F. O. Bryan, and R. A. Tomas, 2017: Scale Dependence of Midlatitude Air–Sea Interaction. *Journal of Climate*, **30 (20)**, 8207–8221, https://doi.org/10.1175/JCLI-D-17-0159.1, URL https://journals.ametsoc.org/view/journals/clim/30/20/jcli-d-17-0159.1.xml, publisher: American Meteorological Society Section: Journal of Climate.

Blackport, R., J. A. Screen, K. van der Wiel, and R. Bintanja, 2019: Minimal influence of reduced Arctic sea ice on coincident cold winters in mid-latitudes. *Nature Climate Change*, **9 (9)**, 697–704, https://doi.org/10.1038/s41558-019-0551-4, URL https://www.nature.com/articles/s41558-019-0551-4, number: 9 Publisher: Nature Publishing Group.

Cattiaux, J., R. Vautard, C. Cassou, P. Yiou, V. Masson-Delmotte, and F. Codron, 2010: Winter 2010 in Europe: A cold extreme in a warming climate. *Geophysical Research Letters*, **37 (20)**, https://doi.org/10.1029/2010GL044613, URL https://onlinelibrary.wiley.com/doi/abs/10.1029/2010GL044613, _eprint: https://onlinelibrary.wiley.com/doi/pdf/10.1029/2010GL044613.

Czaja, A., and C. Frankignoul, 2002: Observed Impact of Atlantic SST Anomalies on the North Atlantic Oscillation. *Journal of Climate*, **15 (6)**, 606–623, https://doi.org/10.

1175/1520-0442(2002)015<0606:OIOASA>2.0.CO;2, URL https://journals.ametsoc.org/view/journals/clim/15/6/1520-0442_2002_015_0606_oioasa_2.0.co_2.xml, publisher: American Meteorological Society Section: Journal of Climate.

Dawson, A., 2016: eofs: A Library for EOF Analysis of Meteorological, Oceanographic, and Climate Data. **4 (1)**, e14, https://doi.org/10.5334/jors.122, URL https://openresearchsoftware.metajnl.com/articles/10.5334/jors.122?utm_source=TrendMD&utm_medium=cpc&utm_campaign=Journal_of_Open_Research_Software_TrendMD_0, number: 1 Publisher: Ubiquity Press.

Deser, C., L. Terray, and A. S. Phillips, 2016: Forced and Internal Components of Winter Air Temperature Trends over North America during the past 50 Years: Mechanisms and Implications. *Journal of Climate*, **29 (6)**, 2237–2258, https://doi.org/10.1175/JCLI-D-15-0304.1, URL https://journals.ametsoc.org/view/journals/clim/29/6/jcli-d-15-0304.1.xml, publisher: American Meteorological Society Section: Journal of Climate.

Deser, C., and M. S. Timlin, 1997: Atmosphere–Ocean Interaction on Weekly Timescales in the North Atlantic and Pacific. *Journal of Climate*, **10 (3)**, 393–408, https://doi.org/10.1175/1520-0442(1997)010<0393:AOIOWT>2.0.CO;2, URL https://journals.ametsoc.org/view/journals/clim/10/3/1520-0442_1997_010_0393_aoiowt_2.0.co_2.xml, publisher: American Meteorological Society Section: Journal of Climate.

Deser, C., R. A. Tomas, and S. Peng, 2007: The Transient Atmospheric Circulation Response to North Atlantic SST and Sea Ice Anomalies. *Journal of Climate*, **20 (18)**, 4751–4767, https://doi.org/10.1175/JCLI4278.1, URL https://journals.ametsoc.org/view/journals/clim/20/18/jcli4278.1.xml, publisher: American Meteorological Society Section: Journal of Climate.

Dong, B., R. T. Sutton, T. Woollings, and K. Hodges, 2013: Variability of the North Atlantic summer storm track: mechanisms and impacts on European climate. *Environmental Research Letters*, **8 (3)**, 034 037, https://doi.org/10.1088/1748-9326/8/3/034037, URL https://dx.doi.org/10.1088/1748-9326/8/3/034037, publisher: IOP Publishing.

Du, Y., and S.-P. Xie, 2008: Role of atmospheric adjustments in the tropical Indian Ocean warming during the 20th century in climate models. *Geophysical Research Letters*, **35 (8)**, https://doi.org/10.1029/2008GL033631, URL https://onlinelibrary.wiley.com/doi/abs/10.1029/2008GL033631, _eprint: https://onlinelibrary.wiley.com/doi/pdf/10.1029/2008GL033631.

Duchon, C. E., 1979: Lanczos Filtering in One and Two Dimensions. *Journal of Applied Meteorology and Climatology*, **18 (8)**, 1016–1022, https://doi.org/10.1175/1520-0450(1979)018<1016:LFIOAT>2.0.CO;2, URL https://journals.ametsoc.org/view/journals/apme/18/8/1520-0450_1979_018_1016_lfioat_2_0_co_2.xml, publisher: American Meteorological Society Section: Journal of Applied Meteorology and Climatology.

Eade, R., D. Smith, A. Scaife, E. Wallace, N. Dunstone, L. Hermanson, and N. Robinson, 2014: Do seasonal-to-decadal climate predictions underestimate the predictability of the real world? *Geophysical Research Letters*, **41 (15)**, 5620–5628, https://doi.org/10.1002/2014GL061146, URL https://onlinelibrary.wiley.com/doi/abs/10.1002/2014GL061146, _eprint: https://onlinelibrary.wiley.com/doi/pdf/10.1002/2014GL061146.

Ferreira, D., and C. Frankignoul, 2005: The Transient Atmospheric Response to Midlatitude SST Anomalies. *Journal of Climate*, **18 (7)**, 1049–1067, https://doi.org/10.1175/JCLI-3313.1, URL https://journals.ametsoc.org/view/journals/clim/18/7/jcli-3313.1.xml, publisher: American Meteorological Society Section: Journal of Climate.

Gastineau, G., F. D'Andrea, and C. Frankignoul, 2013: Atmospheric response to the North Atlantic Ocean variability on seasonal to decadal time scales. *Climate Dynamics*, **40 (9)**, 2311–2330, https://doi.org/10.1007/s00382-012-1333-0, URL https://doi.org/10.1007/s00382-012-1333-0.

Gulev, S. K., M. Latif, N. Keenlyside, W. Park, and K. P. Koltermann, 2013: North Atlantic Ocean control on surface heat flux on multidecadal timescales. *Nature*, **499 (7459)**, 464–467, https://doi.org/10.1038/nature12268, URL https://www.nature.com/articles/nature12268, number: 7459 Publisher: Nature Publishing Group.

Hardiman, S. C., N. J. Dunstone, A. A. Scaife, D. M. Smith, R. Comer, Y. Nie, and H.-L. Ren, 2022: Missing eddy feedback may explain weak signal-to-noise ratios in climate predictions. *npj Climate and Atmospheric Science*, **5 (1)**, 1–8, https://doi.org/10.1038/s41612-022-00280-4, URL https://www.nature.com/articles/s41612-022-00280-4, number: 1 Publisher: Nature Publishing Group.

He, C., A. C. Clement, M. A. Cane, L. N. Murphy, J. M. Klavans, and T. M. Fenske, 2022: A North Atlantic Warming Hole Without Ocean Circulation. *Geophysical Research Letters*, **49 (19)**, e2022GL100 420, https://doi.org/10.1029/2022GL100420, URL https://onlinelibrary.wiley.com/doi/abs/10.1029/2022GL100420, _eprint: https://onlinelibrary.wiley.com/doi/pdf/10.1029/2022GL100420.

Hendon, H. H., and D. L. Hartmann, 1982: Stationary Waves on a Sphere: Sensitivity to Thermal Feedback. *Journal of the Atmospheric Sciences*, **39 (9)**, 1906–1920, https://doi.org/10.1175/1520-0469(1982)039<1906:SWOASS>2.0.CO;2, URL https://journals.ametsoc.org/view/journals/atsc/39/9/1520-0469_1982_039_1906_swoass_2_0_co_2.xml, publisher: American Meteorological Society Section: Journal of the Atmospheric Sciences.

Hersbach, H., and Coauthors, 2020: The ERA5 global reanalysis. *Quarterly Journal of the Royal Meteorological Society*, **146 (730)**, 1999–2049, https://doi.org/10.1002/qj.3803, URL https://onlinelibrary.wiley.com/doi/abs/10.1002/qj.3803, _eprint: https://onlinelibrary.wiley.com/doi/pdf/10.1002/qj.3803.

Hoskins, B. J., and D. J. Karoly, 1981: The Steady Linear Response of a Spherical Atmosphere to Thermal and Orographic Forcing. *Journal of the Atmospheric Sciences*, **38 (6)**, 1179–1196, https://doi.org/10.1175/1520-0469(1981)038<1179:TSLROA>2.0.CO;2, URL https://journals.ametsoc.org/view/journals/atsc/38/6/1520-0469_1981_038_1179_tslroa_2_0_co_2.xml, publisher: American Meteorological Society Section: Journal of the Atmospheric Sciences.

Khatri, H., R. G. Williams, T. Woollings, and D. M. Smith, 2022: Fast and Slow Subpolar Ocean Responses to the North Atlantic Oscillation: Thermal and Dynamical Changes. *Geophysical Research Letters*, **49 (24)**, e2022GL101 480, https://doi.org/10.1029/2022GL101480, URL https://onlinelibrary.wiley.com/doi/abs/10.1029/2022GL101480, _eprint: https://onlinelibrary.wiley.com/doi/pdf/10.1029/2022GL101480.

Knight, J. R., C. K. Folland, and A. A. Scaife, 2006: Climate impacts of the Atlantic Multidecadal Oscillation. *Geophysical Research Letters*, **33 (17)**, https://doi.org/10.1029/2006GL026242, URL https://onlinelibrary.wiley.com/doi/abs/10.1029/2006GL026242, _eprint: https://onlinelibrary.wiley.com/doi/pdf/10.1029/2006GL026242.

Kushnir, Y., W. A. Robinson, I. Bladé, N. M. J. Hall, S. Peng, and R. Sutton, 2002: Atmospheric GCM Response to Extratropical SST Anomalies: Synthesis and Evaluation. *Journal of Climate*, **15 (16)**, 2233–2256, https://doi.org/10.1175/1520-0442(2002)015<2233:AGRTES>2.0.CO;2, URL https://journals.ametsoc.org/view/journals/clim/15/16/1520-0442_2002_015_2233_agrtes_2.0.co_2.xml, publisher: American Meteorological Society Section: Journal of Climate.

Lai, W. K. M., J. I. Robson, L. J. Wilcox, and N. Dunstone, 2022: Mechanisms of Internal Atlantic Multidecadal Variability in HadGEM3-GC3.1 at Two Different Resolutions. *Journal of Climate*, **35 (4)**, 1365–1383, https://doi.org/10.1175/JCLI-D-21-0281.1, URL https://journals.ametsoc.org/view/journals/clim/35/4/JCLI-D-21-0281.1.xml, publisher: American Meteorological Society Section: Journal of Climate.

Lorenz, E. N., 1969: Atmospheric Predictability as Revealed by Naturally Occurring Analogues. *Journal of the Atmospheric Sciences*, **26 (4)**, 636–646, https://doi.org/10.1175/1520-0469(1969)26<636:APARBN>2.0.CO;2, URL https://journals.ametsoc.org/view/journals/atsc/26/4/1520-0469_1969_26_636_aparbn_2_0_co_2.xml, publisher: American Meteorological Society Section: Journal of the Atmospheric Sciences.

Meehl, G. A., and Coauthors, 2021: Initialized Earth System prediction from subseasonal to decadal timescales. *Nature Reviews Earth & Environment*, **2 (5)**, 340–357, https://doi.org/10.1038/s43017-021-00155-x, URL https://www.nature.com/articles/s43017-021-00155-x, number: 5 Publisher: Nature Publishing Group.

Mehta, V. M., M. J. Suarez, J. V. Manganello, and T. L. Delworth, 2000: Oceanic influence on the North Atlantic Oscillation and associated northern hemisphere climate variations: 1959–1993. *Geophysical Research Letters*, **27 (1)**, 121–124, https://doi.org/10.1029/1999GL002381, URL https://onlinelibrary.wiley.com/doi/abs/10.1029/1999GL002381, _eprint: https://onlinelibrary.wiley.com/doi/pdf/10.1029/1999GL002381.

Menary, M. B., D. L. R. Hodson, J. I. Robson, R. T. Sutton, and R. A. Wood, 2015: A Mechanism of Internal Decadal Atlantic Ocean Variability in a High-Resolution Coupled Climate Model. *Journal of Climate*, **28 (19)**, 7764–7785, https://doi.org/10.1175/JCLI-D-15-0106.1, URL https://journals.ametsoc.org/view/journals/clim/28/19/jcli-d-15-0106.1.xml, publisher: American Meteorological Society Section: Journal of Climate.

Menary, M. B., L. C. Jackson, and M. S. Lozier, 2020: Reconciling the Relationship Between the AMOC and Labrador Sea in OSNAP Observations and Climate Models. *Geophysical Research Letters*, **47 (18)**, e2020GL089 793, https://doi.org/10.1029/2020GL089793, URL https://onlinelibrary.wiley.com/doi/abs/10.1029/2020GL089793, _eprint: https://onlinelibrary.wiley.com/doi/pdf/10.1029/2020GL089793.

Menary, M. B., and Coauthors, 2018: Preindustrial Control Simulations With HadGEM3-GC3.1 for CMIP6. *Journal of Advances in Modeling Earth Systems*, **10 (12)**, 3049–3075, https://doi.org/10.1029/2018MS001495, URL https://onlinelibrary.wiley.com/doi/abs/10.1029/2018MS001495, _eprint: https://onlinelibrary.wiley.com/doi/pdf/10.1029/2018MS001495.

Merryfield, W. J., and Coauthors, 2020: Current and Emerging Developments in Subseasonal to Decadal Prediction. *Bulletin of the American Meteorological Society*, **101 (6)**, E869–E896, https://doi.org/10.1175/BAMS-D-19-0037.1, URL https://journals.ametsoc.org/view/journals/bams/101/6/bamsD190037.xml, publisher: American Meteorological Society Section: Bulletin of the American Meteorological Society.

Novak, L., M. H. P. Ambaum, and R. Tailleux, 2015: The Life Cycle of the North Atlantic Storm Track. *Journal of the Atmospheric Sciences*, **72 (2)**, 821–833, https://doi.org/10.1175/JAS-D-14-0082.1, URL https://journals.ametsoc.org/view/journals/atsc/72/2/jas-d-14-0082.1.xml, publisher: American Meteorological Society Section: Journal of the Atmospheric Sciences.

O'Reilly, C. H., D. J. Befort, A. Weisheimer, T. Woollings, A. Ballinger, and G. Hegerl, 2021: Projections of northern hemisphere extratropical climate underestimate internal variability and associated uncertainty. *Communications Earth & Environment*, **2 (1)**, 1–9, https://doi.org/10.1038/s43247-021-00268-7, URL https://www.nature.com/articles/s43247-021-00268-7, number: 1 Publisher: Nature Publishing Group.

O'Reilly, C. H., M. Huber, T. Woollings, and L. Zanna, 2016: The signature of low-frequency oceanic forcing in the Atlantic Multidecadal Oscillation. *Geophysical Research Letters*, **43 (6)**, 2810–2818, https://doi.org/10.1002/2016GL067925, URL https://onlinelibrary.wiley.com/doi/abs/10.1002/2016GL067925, _eprint: https://onlinelibrary.wiley.com/doi/pdf/10.1002/2016GL067925.

O'Reilly, C. H., M. Patterson, J. Robson, P. A. Monerie, D. Hodson, and Y. Ruprich-Robert, 2023: Challenges with interpreting the impact of Atlantic Multidecadal Variability using SST-restoring experiments. *npj Climate and Atmospheric Science*, **6 (1)**, 1–12, https://doi.org/10.1038/s41612-023-00335-0, URL https://www.nature.com/articles/s41612-023-00335-0, number: 1 Publisher: Nature Publishing Group.

O'Reilly, C. H., T. Woollings, and L. Zanna, 2017: The Dynamical Influence of the Atlantic Multidecadal Oscillation on Continental Climate. *Journal of Climate*, **30 (18)**, 7213–7230, https://doi.org/10.1175/JCLI-D-16-0345.1, URL https://journals.ametsoc.org/view/journals/clim/30/18/jcli-d-16-0345.1.xml, publisher: American Meteorological Society Section: Journal of Climate.

O'Reilly, C. H., L. Zanna, and T. Woollings, 2019: Assessing External and Internal Sources of Atlantic Multidecadal Variability Using Models, Proxy Data, and Early Instrumental Indices. *Journal of Climate*, **32 (22)**, 7727–7745, https://doi.org/10.1175/JCLI-D-19-0177.1, URL https://journals.ametsoc.org/view/journals/clim/32/22/jcli-d-19-0177.1.xml, publisher: American Meteorological Society Section: Journal of Climate.

Rodwell, M. J., D. P. Rowell, and C. K. Folland, 1999: Oceanic forcing of the wintertime North Atlantic Oscillation and European climate. *Nature*, **398 (6725)**, 320–323, https://doi.org/10.1038/18648, URL https://www.nature.com/articles/18648, number: 6725 Publisher: Nature Publishing Group.

Årthun, M., and T. Eldevik, 2016: On Anomalous Ocean Heat Transport toward the Arctic and Associated Climate Predictability. *Journal of Climate*, **29 (2)**, 689–704, https://doi.org/10.1175/JCLI-D-15-0448.1, URL https://journals.ametsoc.org/view/journals/clim/29/2/jcli-d-15-0448.1.xml, publisher: American Meteorological Society Section: Journal of Climate.

Årthun, M., T. Eldevik, E. Viste, H. Drange, T. Furevik, H. L. Johnson, and N. S. Keenlyside, 2017: Skillful prediction of northern climate provided by the ocean. *Nature Communications*, **8 (1)**, 15 875, https://doi.org/10.1038/ncomms15875, URL https://www.nature.com/articles/ncomms15875, number: 1 Publisher: Nature Publishing Group.

Scaife, A. A., and D. Smith, 2018: A signal-to-noise paradox in climate science. *npj Climate and Atmospheric Science*, **1 (1)**, 1–8, https://doi.org/10.1038/s41612-018-0038-4, URL https://www.nature.com/articles/s41612-018-0038-4, number: 1 Publisher: Nature Publishing Group.

Scaife, A. A., and Coauthors, 2019: Does increased atmospheric resolution improve seasonal climate predictions? *Atmospheric Science Letters*, **20 (8)**, e922, https://doi.org/10.1002/asl.922, URL https://onlinelibrary.wiley.com/doi/abs/10.1002/asl.922, _eprint: https://onlinelibrary.wiley.com/doi/pdf/10.1002/asl.922.

Simpson, I. R., C. Deser, K. A. McKinnon, and E. A. Barnes, 2018: Modeled and Observed Multidecadal Variability in the North Atlantic Jet Stream and Its Connection to Sea Surface Temperatures. *Journal of Climate*, **31 (20)**, 8313–8338, https://doi.org/10.1175/JCLI-D-18-0168.1, URL https://journals.ametsoc.org/view/journals/clim/31/20/jcli-d-18-0168.1.xml, publisher: American Meteorological Society Section: Journal of Climate.

Smith, D. M., and Coauthors, 2020: North Atlantic climate far more predictable than models imply. *Nature*, **583 (7818)**, 796–800, https://doi.org/10.1038/s41586-020-2525-0, URL https://www.nature.com/articles/s41586-020-2525-0, number: 7818 Publisher: Nature Publishing Group.

Sutton, R. T., and B. Dong, 2012: Atlantic Ocean influence on a shift in European climate in the 1990s. *Nature Geoscience*, **5 (11)**, 788–792, https://doi.org/10.1038/ngeo1595, URL https://www.nature.com/articles/ngeo1595, number: 11 Publisher: Nature Publishing Group.

Sutton, R. T., and D. L. R. Hodson, 2007: Climate Response to Basin-Scale Warming and Cooling of the North Atlantic Ocean. *Journal of Climate*, **20 (5)**, 891–907, https://doi.org/10.1175/JCLI4038.1, URL https://journals.ametsoc.org/view/journals/clim/20/5/jcli4038.1.xml, publisher: American Meteorological Society Section: Journal of Climate.

Titchner, H. A., and N. A. Rayner, 2014: The Met Office Hadley Centre sea ice and sea surface temperature data set, version 2: 1. Sea ice concentrations. *Journal of Geophysical Research: Atmospheres*, **119 (6)**, 2864–2889, https://doi.org/10.1002/2013JD020316, URL https://onlinelibrary.wiley.com/doi/abs/10.1002/2013JD020316, _eprint: https://onlinelibrary.wiley.com/doi/pdf/10.1002/2013JD020316.

van den Dool, H., J. Huang, and Y. Fan, 2003: Performance and analysis of the constructed analogue method applied to U.S. soil moisture over 1981–2001. *Journal of Geophysical Research: Atmospheres*, **108 (D16)**, https://doi.org/10.1029/2002JD003114, URL https://onlinelibrary.wiley.com/doi/abs/10.1029/2002JD003114, _eprint: https://onlinelibrary.wiley.com/doi/pdf/10.1029/2002JD003114.

van den Dool, H. M., 1994: Searching for analogues, how long must we wait? *Tellus A: Dynamic Meteorology and Oceanography*, **46 (3)**, 314–324, https://doi.org/10.3402/tellusa.v46i3.15481, URL http://a.tellusjournals.se/article/10.3402/tellusa.v46i3.15481/, number: 3 Publisher: Stockholm University Press.

Wallace, J. M., Q. Fu, B. V. Smoliak, P. Lin, and C. M. Johanson, 2012: Simulated versus observed patterns of warming over the extratropical Northern Hemisphere continents during the cold season. *Proceedings of the National Academy of Sciences*, **109 (36)**, 14 337–14 342, https://doi.org/10.1073/pnas.1204875109, URL https://www.pnas.org/doi/full/10.1073/pnas.1204875109, publisher: Proceedings of the National Academy of Sciences.

Williams, K. D., and Coauthors, 2018: The Met Office Global Coupled Model 3.0 and 3.1 (GC3.0 and GC3.1) Configurations. *Journal of Advances in Modeling Earth Systems*, **10 (2)**, 357–380, https://doi.org/10.1002/2017MS001115, URL https://onlinelibrary.wiley.com/doi/abs/10.1002/2017MS001115, _eprint: https://onlinelibrary.wiley.com/doi/pdf/10.1002/2017MS001115.

Wills, S. M., D. W. J. Thompson, and L. M. Ciasto, 2016: On the Observed Relationships between Variability in Gulf Stream Sea Surface Temperatures and the Atmospheric Circulation over the North Atlantic. *Journal of Climate*, **29 (10)**, 3719–3730, https://doi.org/10.1175/JCLI-D-15-0820.1, URL https://journals.ametsoc.org/view/journals/clim/29/10/jcli-d-15-0820.1.xml, publisher: American Meteorological Society Section: Journal of Climate.

Zhang, R., R. Sutton, G. Danabasoglu, Y.-O. Kwon, R. Marsh, S. G. Yeager, D. E. Amrhein, and C. M. Little, 2019: A Review of the Role of the Atlantic Meridional Overturning Circulation in Atlantic Multidecadal Variability and Associated Climate Impacts. *Reviews of Geophysics*, **57 (2)**, 316–375, https://doi.org/10.

1029/2019RG000644, URL https://onlinelibrary.wiley.com/doi/abs/10.1029/2019RG000644, _eprint: https://onlinelibrary.wiley.com/doi/pdf/10.1029/2019RG000644.